





Maximal superconductivity in proximity to the charge density wave quantum critical point in Cu_xTiSe_2

Tae-Ho Park ^{*} and Obinna P. Uzoh *Department of Physics, Sungkyunkwan University, Suwon 16419, Korea*Han-Yong Choi [†]*Department of Physics, Sungkyunkwan University, Suwon 16419, Korea
and Asia Pacific Center for Theoretical Physics, Pohang 37673, Korea* (Received 11 August 2021; revised 25 October 2021; accepted 26 October 2021; published 10 November 2021)

Superconductivity emerges in $1T\text{-TiSe}_2$ when its charge density wave (CDW) order is suppressed by Cu intercalation or pressure. Since the CDW state is thought to be an excitonic insulator, an interesting question is whether the superconductivity is also mediated by excitonic fluctuations. We investigated this question as to the nature of doping induced superconductivity in Cu_xTiSe_2 by asking about its consistency with the phonon-mediated pairing. We employed the *ab initio* density functional theory and density functional perturbation theory to compute the electron-phonon coupling Eliashberg function from which to calculate the superconducting (SC) critical temperature T_c . The calculated T_c as a function of the doping concentration x exhibits a dome shape with the maximum T_c of 2–6 K at $x \approx 0.05$ for the Coulomb pseudopotential $0 \leq \mu^* \leq 0.1$. The maximal T_c was found to be pinned to the quantum critical point where the CDW is completely suppressed and the corresponding phonon mode becomes soft. Underlying physics is that the reduced phonon frequency enhances the electron-phonon coupling constant λ , which overcompensates the frequency decrease to produce a net increase of T_c . The doping induced superconductivity in Cu_xTiSe_2 seems to be consistent with the phonon-mediated pairing. A comparative discussion was made with the pressure induced superconductivity in TiSe_2 .

DOI: [10.1103/PhysRevB.104.184506](https://doi.org/10.1103/PhysRevB.104.184506)

I. INTRODUCTION

The interplay between superconductivity and other orders in proximity such as antiferromagnetism, nematicity, and CDW has been one of engaging research topics in condensed matter physics [1–5]. Despite their diversity in crystal structure and phenomenology, vast classes of superconductors including the copper oxides [6], Fe based superconductors [7,8], heavy fermion materials [9,10], and transition metal dichalcogenides (TMDC) [11] exhibit the common trait that the SC critical temperature T_c shows a dome shape as the tuning parameters like the chemical concentration, pressure, and external field are varied. The maximum T_c appears close to a quantum critical point (QCP) where one of the neighboring orders is completely suppressed as a tuning parameter is varied. This is reminiscent of quantum critical superconductivity, which posits that the very interaction underlying the neighboring order also induces superconductivity. The recurrence of this “universal phase diagram” suggests a deep connection between superconductivity and neighboring orders [6].

TMDC materials MX_2 , where $M = \text{Nb, Ti, Ta, Mo}$, and $X = \text{Se, S}$, exhibit this phase diagram from the interplay between superconductivity and CDW order [11–15]. Of particular interest is $1T\text{-TiSe}_2$ because its CDW is thought to

be induced by the exciton condensation of electron-hole pairs [16]. The $1T\text{-TiSe}_2$ is a TMDC semiconductor/semimetal of a layered structure with an indirect gap/overlap between the Se $4p$ hole band centered at the Γ point and the Ti $3d$ electron bands around the L points in the Brillouin zone (BZ) as shown in Fig. 1. An exciton, a bound state of an electron from the L_i band and a hole from the Γ band in Fig. 1(b), then has a nonzero net momentum and the inverse of the momentum sets a new length scale. Consequently, the exciton condensation is accompanied by a structural instability at the inverse momentum and makes a phase transition to a CDW of $2 \times 2 \times 2$ superstructure below the critical temperature $T^{\text{CDW}} \approx 200$ K [16].

The CDW is suppressed by Cu intercalation, pressure, or electric field and superconductivity emerges. The SC critical temperature T_c exhibits a dome shape as a function of the Cu concentration x or the pressure P . As for the Cu intercalation, T_c reaches maximum of 3.79–4.15 K at $x_{\text{opt}} \approx 0.077\text{--}0.08$ in close proximity to the QCP of $x_c \approx 0.06\text{--}0.07$ at which the CDW is completely suppressed [11,17]. Also, Raman scattering experiments showed the frequency softening and divergent linewidth of the CDW amplitude mode corresponding to the L point as x approaches x_c [18,19]. These seem in accord with the quantum critical superconductivity alluded above which suggests that the very interaction underlying the CDW formation may also induce the superconductivity in Cu_xTiSe_2 . An alternative view is that the proximity of CDW and SC is coincidental and the superconductivity is a phonon-mediated conventional one [20].

^{*}thpark@skku.edu[†]hychoi@skku.edu

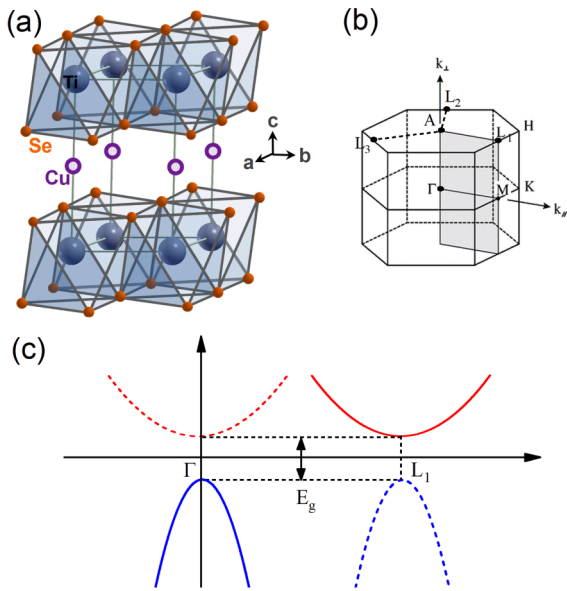


FIG. 1. (a) Crystal structure of Cu_xTiSe_2 illustrating the intercalated Cu atoms between TiSe_2 layers. (b) 1st BZ of 1T- TiSe_2 corresponding to the crystal structure of (a). (c) Energy dispersion of the hole and electron bands along the $\Gamma - L_1$ direction. The hole band around the Γ and three electron bands around L_i points are shown in blue and red, respectively. E_g is the indirect gap between the electron and hole bands. BZ is reduced in the CDW phase and the backfolded dispersions appear as shown in the blue- and red-dashed lines.

As to the pressure, Kusmartseva *et al.* observed by transport measurements that superconductivity appears in the range of $P \approx 2-4$ GPa and the maximum $T_c \approx 1.8$ K occurs around $P_{\text{opt}} \approx 3$ GPa close to the CDW suppression [12]. However, Joe *et al.* [21] and Kitou *et al.* [17] observed with the synchrotron x-ray diffraction on single crystals that the P induced suppression is at $P_c \approx 5.1$ GPa, which is more than 1 GPa beyond the end of the SC region. Joe *et al.* also observed that a reentrant incommensurate CDW phase appeared near the P_{opt} above the SC dome, which seemed to indicate that the pressure induced superconductivity in TiSe_2 may not be connected to the CDW suppression but to the CDW domain walls. Calandra and Mauri showed with the *ab initio* calculations that the behavior of T_c as a function of pressure is entirely determined by the electron-phonon interaction without a need for invoking exciton mechanism [22].

For intercalated Cu_xTiSe_2 , Zhao *et al.* [20] and Qian *et al.* [23] observed with ARPES experiments that the Cu doping raises the chemical potential from inside the semiconducting gap at zero doping to the Ti 3d electron band. This of course leads to the enhanced electronic density of states (DOS) and the increased screening, which enhance superconductivity and weaken exciton condensation, respectively. These are the two different effects of the doping by which the authors argued that the seeming competition between CDW and SC is coincidental. Li *et al.* measured the in-plane thermal conductivity as a function of temperature for Cu_xTiSe_2 at $x = 0.06$ and concluded that it is a conventional s -wave single gap superconductor [24]. Kogar *et al.* performed x-ray diffraction experiments on Cu_xTiSe_2 and proposed that the

incommensuration and domain walls of the CDW may play a crucial role in the formation of the SC state as in the pressure induced SC mentioned above [25].

On the other hand, Kitou *et al.* [17] and Maschek *et al.* [26] stressed the dissimilarity between the doping induced and pressure induced cases. For instance, Maschek *et al.* argued that the doping induced SC can be understood by the phonon mediated pairing mechanism alone while a hybridization of phonon and exciton modes is necessary for the pressure induced SC. The possibility of an unconventional s_{\pm} pairing between the electron and incipient hole bands and the time-reversal-symmetry breaking chiral superconductivity has also been proposed out of the interplay between CDW and pairing [27] (see below).

Here, we demonstrate that the superconducting T_c as a function of the Cu intercalation concentration x for Cu_xTiSe_2 is determined by the electron-phonon interaction based on the *ab initio* density functional theory (DFT) and density functional perturbation theory (DFPT) calculations, which consider the Cu intercalation explicitly. From these calculations, the maximal T_c was found to be pinned to the minimum phonon frequency. This naturally leads to the dome shape of T_c as a function of an external parameter as has been observed and discussed in many classes of materials [1,28]. Underlying physics will be discussed after the presentation of the calculations. We argue that superconductivity in Cu_xTiSe_2 is a phonon mediated conventional pairing and the proximity of the maximal T_c and CDW quantum critical point is not coincidental.

II. COMPUTATIONAL DETAILS

We performed all electronic and phonon computations using first-principles methods within the QUANTUM ESPRESSO suite [29], implementing the DFT. For the exchange-correlation contribution to the total energy, we used the local density approximation (LDA) functional in the parametrization of Perdew-Zunger [30]. For all the systems calculated, the lattice parameters were fixed to the experimentally observed values obtained in Ref. [11] and the atomic positions were then allowed to fully relax until the forces on the atoms became less than 10^{-5} Ry/a.u. In the electronic structure calculations, core electrons were treated with the optimized norm-conserving Vanderbilt pseudopotentials [31], while the Ti $3s^2 3p^6 4s^2 3d^2$ and Se $3d^{10} 4s^2 4p^4$ were treated as valence electrons and was described with plane waves up to a kinetic energy cutoff of 70 Ry. The BZ of the primitive cell was sampled with a $24 \times 24 \times 24$ Monkhorst-Pack [32] \mathbf{k} -point grid using a Marzari-Vanderbilt [33] smearing of 0.01 Ry.

To take the doping effects into consideration for Cu_xTiSe_2 , we utilized the virtual crystal approximation (VCA) technique [34,35]. In the VCA, the system under study is computed in the primitive periodicity of the crystal with a virtual atom that interpolates between two constituent atoms. It is computationally much less expensive in comparison with, for example, the supercell approach, which requires very large supercells [36]. Within a pseudopotential approach to DFT, the pseudopotential V_{ps}^{VA} for a virtual atom can be constructed by a simple superposition of the pseudopotentials V_{ps}^A and V_{ps}^B of two atoms

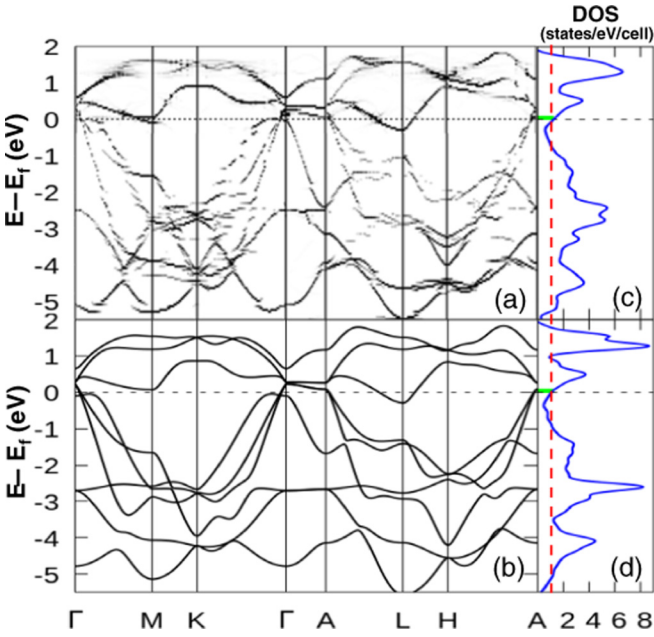


FIG. 2. (a) Electronic band structures of unfolded $3 \times 3 \times 1$ supercell $\text{Cu}_{0.11}\text{TiSe}_2$, and (b) VCA $\text{Li}_{0.11}\text{TiSe}_2$. (c) Electronic DOS for the supercell system with the green area around the Fermi level corresponding to the amount of electrons transferred from the Cu cations to the TiSe_2 layers, and (d) DOS for the VCA system with the green area corresponding to the amount of electrons transferred from the virtual Li cations to the TiSe_2 layers. The vertical (red dashed) line is a guide to eyes to compare DOS at the Fermi level for a supercell to VCA calculations.

A and B as [34,35]

$$V_{ps}^{VA} = xV_{ps}^A + (1-x)V_{ps}^B. \quad (1)$$

However, using Cu atom within VCA to reproduce the electronic structure of more accurate supercell calculations is problematic, as was also reported in Ref. [37]. Cu outer $4s$ orbital participates in the electron doping of TMDC materials [36,38], and the Cu $3d$ electrons are irrelevant in the electronic structure near the Fermi level. Sawa *et al.* demonstrated that virtual Li atom can successfully simulate the Cu doping because Li has one electron in the s outer shell like Cu within the VCA technique [37]. Following this, we constructed virtual pseudopotentials by mixing Li and He norm-conserving pseudopotentials as in Eq. (1).

To validate our VCA modeled Li_xTiSe_2 system, we performed calculations for a $3 \times 3 \times 1$ supercell Cu-intercalated TiSe_2 . This corresponds to the Cu doping of $x = 0.11$. The electronic structure was subsequently calculated and unfolded using the procedure of Refs. [39,40]. These unfolded supercell electronic bands were then compared with the VCA calculations for Li_xTiSe_2 at $x = 0.11$; Figs. 2(a) and 2(b) show the comparison between them. The good agreement of their dispersions around the Fermi level provides a justification of the VCA. Also, the electron DOS for the supercell and VCA, as shown in Figs. 2(c) and 2(d), are in good agreement with each other around the Fermi level and also with the previous calculations [36]. The number of doped electrons per unit cell, which is the charge transferred from the cation to the

TiSe_2 layers, can be calculated by integrating the DOS for the shifted chemical potential from doping with respect to the Fermi level of the pristine TiSe_2 . We found that the same number of electrons ($x = 0.11$) per unit cell for both VCA and supercell calculations as shown by the green shaded areas in Figs. 2(c) and 2(d).

For the calculations of the phonon modes of the cation intercalated TiSe_2 , we replaced the Li ion mass with that of Cu. We then employed DFPT in the linear response [41] to calculate the dynamical matrices with $2 \times 2 \times 2$ \mathbf{q} -points grid from which to calculate the eigenfrequencies, eigenmodes, and the interatomic force constants. Then the electron-phonon coupling quantities were calculated on a significantly finer grid using the electron-phonon Wannier (EPW) interpolation scheme [42,43]. The electronic wave functions required for the Wannier-Fourier interpolation were calculated on a uniform and Γ centered \mathbf{k} mesh of size $12 \times 12 \times 12$. For the maximally localized Wannier orbitals, these six Ti d_{xy} , d_{xz} , d_{yz} and Se p_x , p_y , p_z states were considered. The electron-phonon matrix elements were first computed on a coarse $24 \times 24 \times 24$ \mathbf{k} mesh and $2 \times 2 \times 2$ \mathbf{q} mesh. Then, it was interpolated to a finer $40 \times 40 \times 40$ \mathbf{k} mesh and a $20 \times 20 \times 20$ \mathbf{q} mesh.

Ideally, it is desirable we make a similar comparison between the Li-VCA and Cu supercell calculations for the phonon dispersion. This, however, is extremely demanding and the very reason for employing the VCA is to avoid these costly phonon calculations. One may expect that the VCA phonon results would be acceptable in that the DFT electronic structures are correctly reproduced by the VCA as presented in Fig. 2, and the DFPT phonon calculations are the DFT up to the second order of the infinitesimal ionic displacements.

The phonon frequencies $\omega_{\mathbf{q}\nu}$ as a function of the phonon wave vector \mathbf{q} for a given phonon mode ν are calculated by solving the eigenvalue equation,

$$\text{Det}|D_{IJ}^{\alpha\beta}(\mathbf{q}, \nu) - \omega_{\mathbf{q}\nu}^2| = 0. \quad (2)$$

$D_{IJ}^{\alpha\beta}(\mathbf{q}, \nu)$ is the dynamical matrix defined as

$$D_{IJ}^{\alpha\beta}(\mathbf{q}, \nu) = \frac{1}{\sqrt{M_I M_J}} \frac{\partial^2 E_{\text{tot}}}{\partial u_I^\alpha(\mathbf{q}, \nu) \partial u_J^\beta(\mathbf{q}, \nu)}, \quad (3)$$

where E_{tot} is the total energy of the system and $u_I^\alpha(u_J^\beta)$ is the displacement of atom $I(J)$ in direction $\alpha(\beta)$, and $M_I(M_J)$ denotes the atomic mass.

For a three-dimensional material with N_a atoms per unit cell, the number of phonon modes is $3N_a$ and the dynamical matrix becomes $3N_a \times 3N_a$ matrix for \mathbf{q} and ν . This requires that the integral of the phonon DOS over frequency be equal to 9 for TiSe_2 and $3(3+x)$ for Cu_xTiSe_2 . This is written in terms of the phonon DOS $F(\omega)$ as

$$\int_0^\infty d\omega F(\omega) = 3(3+x). \quad (4)$$

But, because the Cu intercalation was modelled using the virtual atom, a unit cell has 4 atoms and there exist 12 phonon modes for any nonzero doping. To satisfy the requirement of Eq. (4), the standard form of the phonon DOS

$$F(\omega) = \sum_\nu \int_{\text{BZ}} \frac{d\mathbf{q}}{\Omega_{\text{BZ}}} \delta(\omega - \omega_{\mathbf{q}\nu}) \quad (5)$$

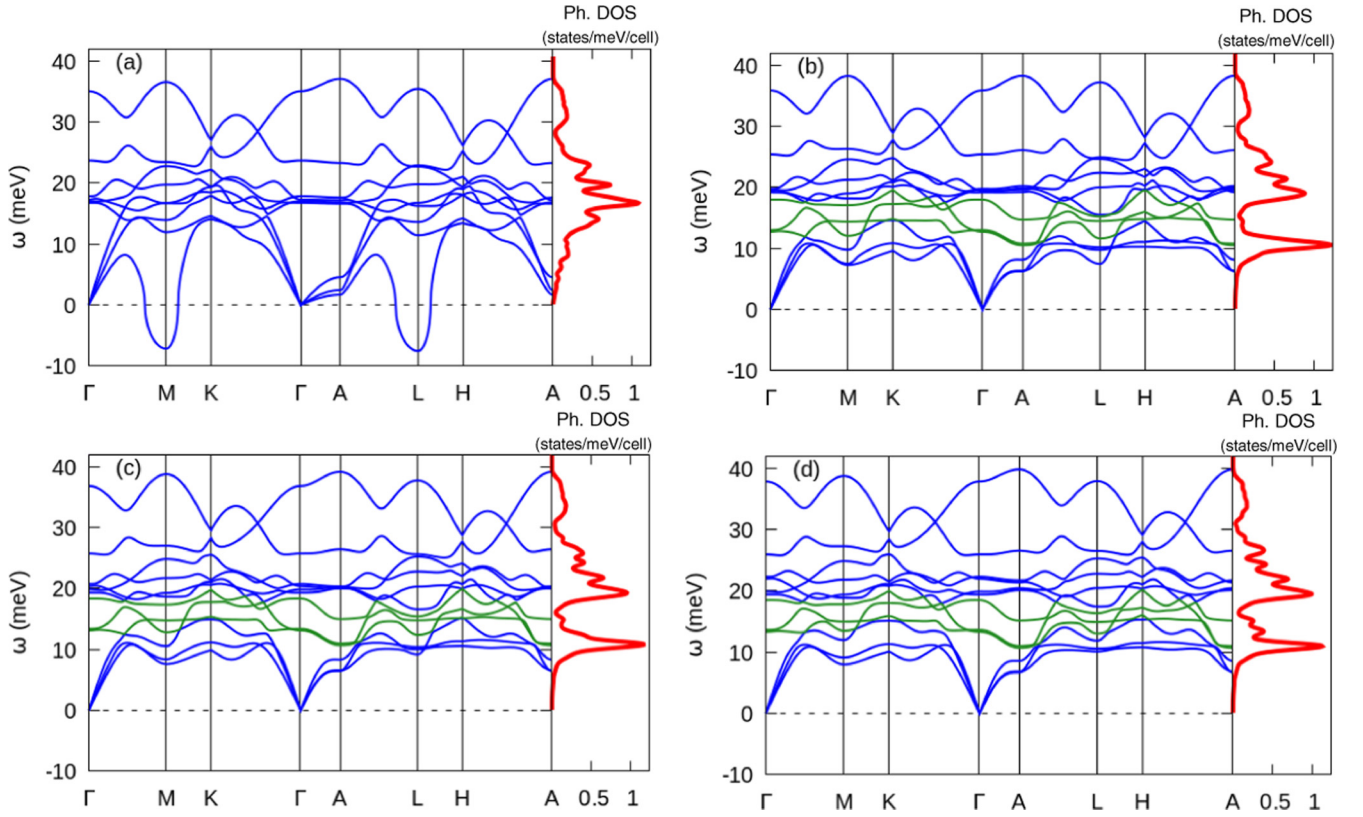


FIG. 3. The phonon dispersions and corresponding phonon density of states for Cu_xTiSe_2 at $x = 0, 0.05, 0.08,$ and 0.15 are shown, respectively, in (a), (b), (c), and (d). The dopant induced phonon modes appear in between the acoustic and optical modes and are shown by green colored lines.

was extended to

$$F(\omega) = \sum_v \int_{\text{BZ}} \frac{d\mathbf{q}}{\Omega_{\text{BZ}}} \delta(\omega - \omega_{\mathbf{q}v}) \sum_{j=1}^{N_{\text{ph}}} a_{jv}^2 \beta_j. \quad (6)$$

$N_{\text{ph}} = 12$ is the number of phonon modes, a_{jv} is the j th component of the eigenvector corresponding to the frequency $\omega_{\mathbf{q}v}$, and β_j equals the concentration x when j refers to the virtual atom and equals 1 otherwise. Then, Eq. (4) is guaranteed using the normalization condition $\sum_v a_{jv}^2 = 1$.

The electron-phonon matrix element for the scattering of an electron in band n at wave vector \mathbf{k} to a state in band m with wave vector $\mathbf{k}+\mathbf{q}$ by a phonon is given by

$$g_{mn}^v(\mathbf{k}, \mathbf{q}) = \left(\frac{\hbar}{2M\omega_{\mathbf{q}v}} \right)^{1/2} \langle m, \mathbf{k} + \mathbf{q} | \delta_{\mathbf{q}v} V_{\text{SCF}} | n, \mathbf{k} \rangle. \quad (7)$$

In this expression, $|n, \mathbf{k}\rangle$ is the bare electronic Bloch state, $\omega_{\mathbf{q}v}$ is the screened phonon frequency, M is the ionic mass, and $\delta_{\mathbf{q}v} V_{\text{SCF}}$ is the derivative of the self-consistent potential with respect to a collective ionic displacement corresponding to phonon wave vector \mathbf{q} and mode v .

The Eliashberg function $\alpha^2 F(\omega)$ is given by [44]

$$\begin{aligned} \alpha^2 F(\omega) &= N(\epsilon_F) \sum_{m,n,v} \iint_{\text{BZ}} \frac{d\mathbf{k}}{\Omega_{\text{BZ}}} \frac{d\mathbf{q}}{\Omega_{\text{BZ}}} |g_{mn}^v(\mathbf{k}, \mathbf{q})|^2 \\ &\times \frac{\delta(\epsilon_{m,\mathbf{k}+\mathbf{q}} - \epsilon_F)}{N(\epsilon_F)} \frac{\delta(\epsilon_{n,\mathbf{k}} - \epsilon_F)}{N(\epsilon_F)} \delta(\omega - \omega_{\mathbf{q}v}) \\ &\times \sum_{j=1}^{12} a_{jv}^2 \beta_j, \end{aligned} \quad (8)$$

where $N(\epsilon_F)$ is the density of states at Fermi level per unit cell and per spin. The dimensionless coupling constant λ is given by the integral

$$\lambda = 2 \int_0^\infty \frac{d\omega}{\omega} \alpha^2 F(\omega). \quad (9)$$

The SC critical temperature T_c is computed by the Allen-Dynes-McMillan formula [45,46]:

$$T_c = \frac{\langle \omega_{\text{ln}} \rangle}{1.2} \exp \left[\frac{-1.04(1 + \lambda)}{\lambda - \mu^*(1 + 1.062\lambda)} \right], \quad (10)$$

where the logarithmic average of phonon frequency is

$$\langle \omega_{\text{ln}} \rangle = \exp \left[\frac{2}{\lambda} \int \frac{d\omega}{\omega} \alpha^2 F(\omega) \log \omega \right], \quad (11)$$

and μ^* is the Coulomb pseudopotential. Recall that the two important parameters λ and $\langle \omega_{\text{ln}} \rangle$ to determine T_c are not independent but are related with each other as given by Eqs. (9) and (11).

III. RESULTS AND DISCUSSION

We show in Fig. 3 the phonon dispersions for pristine TiSe_2 and doped Li_xTiSe_2 systems representative of Cu_xTiSe_2 . For the pristine case of Fig. 3(a) the phonon dispersion exhibits the imaginary frequencies (shown as negative frequencies) near the M and L points. This indicates the instability toward the $2 \times 2 \times 2$ superstructure mentioned in the Introduction. Figures 3(b), 3(c), and 3(d) show the phonon dispersions for $x =$

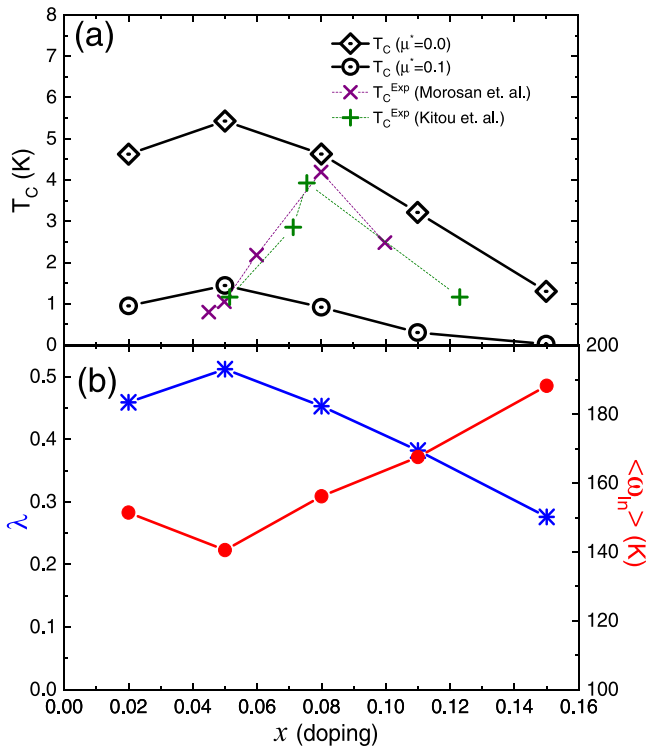


FIG. 4. (a) SC critical temperature T_c for $\mu^* = 0.0$ (\diamond) and $\mu^* = 0.1$ (\odot) together with experimental T_c from Ref. [11] (purple \times) and Ref. [17] (green $+$) and (b) logarithmic average of phonon frequency $\langle \omega_{in} \rangle$ (red \bullet) and electron-phonon coupling constant λ (blue $*$), as a function of doping concentration x in Cu_xTiSe_2 .

0.05, 0.08, and 0.11, respectively. The dopant induced phonon modes appear in between the acoustic and optical modes as shown in green lines in the figures. The doping concentration x was taken into consideration in the T_c calculations via the β_j factor in the Eliashberg function of Eq. (8).

We show in Fig. 4(a) the superconducting T_c against the experimental measurements from Morosan *et al.* [11] and from Kitou *et al.* [17] as a function of x , and in Fig. 4(b) the corresponding dimensionless electron-phonon coupling constant λ and logarithmically averaged phonon frequency $\langle \omega_{in} \rangle$. These were calculated using the Eliashberg function shown in Fig. 5 and Eqs. (9)–(11). Although the calculated doping concentration at the maximum T_c ($x \approx 0.05 \pm 0.01$) is slightly lower than the experimental value ($x \approx 0.077$ – 0.08) due to the overestimated doping effect by the LDA exchange functional [36] and VCA technique, our results reproduce the T_c close to the experimental values and the observed superconducting T_c dome shape as reported in Refs. [11,17]. For the weak coupling superconductors of $\lambda \lesssim 1$, the Allen-Dynes-McMillan formula T_c is very close to the T_c from solutions of the Eliashberg equation [44]. The obtained λ as shown in Fig. 4(b) is about 0.5 or smaller. Maschek *et al.* simulated the doping induced CDW suppression and SC in the DFT and DFPT calculations by tuning the smearing parameter σ , which is often considered as the electronic temperature scale, as the CDW instability was suppressed at $\sigma = 150$ meV as σ was varied. They reported $\lambda \approx 1$ at the CDW suppression, which is about twice larger than the present calculations. This

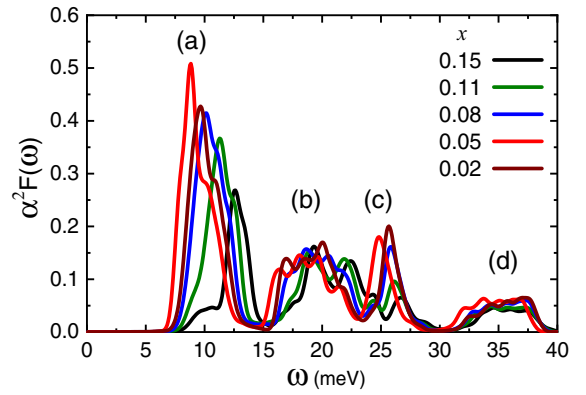


FIG. 5. The Eliashberg function $\alpha^2 F(\omega)$ calculated using EPW at the dopings indicated in the inset. [(a)–(d)] indicate the phonon modes analyzed in Fig. 6.

discrepancy probably comes from the different values of σ and different treatment of the doping. We took $\sigma = 10$ meV. In the current calculations we explicitly included the dopants in the calculations, which suppress the CDW instability and there was no need to tune the smearing parameter to large values.

The maximum T_c as a function of x is pinned to the minimum phonon frequency as has been observed and discussed in many classes of materials [1,28]. The reduced phonon frequency enhances λ due to the ω factor in the denominator of Eq. (9). Recall that a reduced frequency decreases the T_c from the viewpoint of BCS T_c formula. But the enhanced λ overcompensates the frequency decrease to produce a net increase of T_c . From a more general viewpoint, which is valid for the strong coupling T_c as well, we have

$$T_c \sim \sqrt{\omega_0^2 - \omega_{ph}^2}, \quad (12)$$

where ω_0 and ω_{ph} are, respectively, the bare and renormalized phonon frequency [28]. T_c is maximum when ω_{ph} is minimum. As doping is increased or decreased away from the optimal concentration, the phonon frequency hardens back and λ is decreased to yield a reduced T_c . This results in a dome shape of T_c as a function of x in Cu_xTiSe_2 . When λ becomes comparable with the Coulomb pseudopotential μ^* , superconductivity is completely suppressed, which is around $x \approx 0.15$ for $\mu^* = 0.1$ without the doping induced scattering enhancement as x increases [20].

This discussion can be seen more explicitly in Fig. 5, which shows the electron-phonon coupling Eliashberg function $\alpha^2 F(\omega)$ for the doping concentration $x = 0.02, 0.05, 0.08, 0.11$, and 0.15 . The $\alpha^2 F(\omega)$ displays four groups of modes as labeled as (a), (b), (c), and (d) in the figure. The most significant variation of $\alpha^2 F(\omega)$ as a function of x is the peak position and strength of mode (a). It exhibits the lowest frequency and largest strength at $x = 0.05$ to give the highest T_c .

The character of the modes is shown in Fig. 6. The mode Fig. 6(a), also labeled as (a) in Fig. 5, is characterized by the in-plane dopant ion and Se ion vibrations. This is the combination of the longitudinal acoustic and the first dopant optical mode [47]. It contributes about 2/3 of the total λ

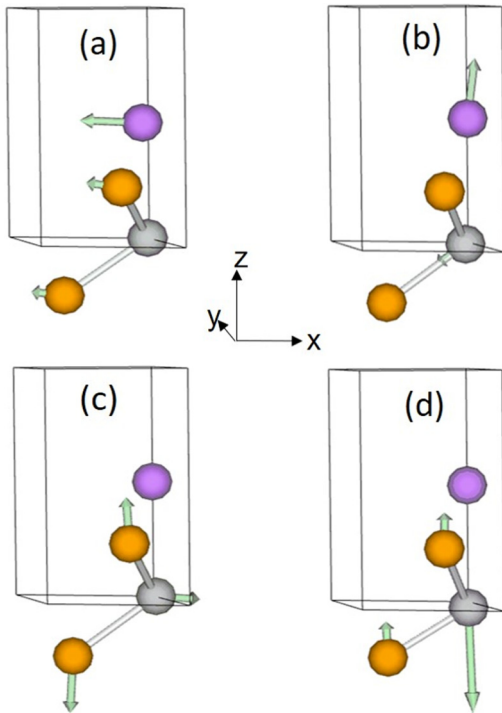


FIG. 6. The analysis of the phonon modes contributing to superconductivity. The labels (a)–(d) correspond to the modes of Fig. 5. The grey, yellow, and purple balls represent the Ti, Se, and virtual Li atoms, respectively. The green arrows represent the direction of the vibration motion of atoms.

and is the dominant phonon mode contributing to the superconductivity. The (b) phonon mode is a combination of the out-of-plane dopant optical mode and Ti transverse optical mode [48]. These modes of (a) and (b) involving the dopant ions would not have been captured in the calculations, for example, using the rigid shift of the Fermi energy. The phonon mode (c) is characterized by the combination of the out-of-plane Se and the in-plane Ti displacements. This mode dominantly comes from the longitudinal optical phonon mode [47,49]. Finally, the phonon mode (d) in the high energy region is the out-of-plane longitudinal optical mode of the out-of-phase Ti and Se ions [50].

We have presented that the doping induced SC in Cu_xTiSe_2 may be understood in terms of the phonon mediated pairing. The maximal T_c was pinned to the CDW QCP at which the phonon frequency is minimum and λ is maximum. On the other hand, the pressure induced SC seems at odds with this picture, although there are reports that this can also be understood within the phonon mediated pairing [22]. The CDW is completely suppressed, that is, $T^{\text{CDW}} = 0$ if the normal state gap E_g is larger than the exciton binding energy in the excitonic insulator picture. The exciton condensation driven CDW is also suppressed by a Lifshitz transition (that is, $E_g = 0$) reported by Bok *et al.* from their material specific calculations [51]. Accepting that E_g is positive (semiconducting) at the ambient pressure for TiSe_2 , the pressure induced QCP at $P_c \approx 5.1$ GPa suggests that $E_g = 0$ at $P = P_c$ and $E_g > 0$ for $P < P_c$.

The superconductivity for $2 \lesssim P \lesssim 4$ GPa then emerges out of a semiconducting normal state. This can be the s_{\pm} SC state suggested by Ganesh *et al.* if samples are accidentally doped, for example, by crystal imperfections [27]. On the other hand, Maschek *et al.* argued that the hybridization between the phonon and exciton modes pushes the critical point of the hybrid mode up but T_c maximum is below the QCP. This, however, does not seem to be supported by the recent paper by Lee *et al.* [52]. They reported that a SC dome appears centered at the tunable QCP by both the Cu concentration and pressure. Alternatively, if the incommensurate CDW intervenes before the CDW is completely suppressed as reported by Kogar *et al.* for Cu intercalation [25] and by Joe *et al.* for the pressure [21], the incommensurateness is accommodated by forming the domain walls. Then SC may emerge out of the domain wall metallic state via phonon mediated pairing for both doping and pressure induced cases. It seems highly desirable that the experimental phase diagram in the doping and pressure parameter space is more accurately delineated with regard to the commensurate and incommensurate CDW phases.

IV. SUMMARY AND CONCLUDING REMARKS

In this paper, we demonstrated that the superconducting T_c as a function of the Cu intercalation concentration x for Cu_xTiSe_2 is entirely determined by the electron-phonon interaction without a necessity to invoke the exciton mechanism. We employed the *ab initio* density functional theory and density functional perturbation theory to calculate the electron-phonon coupling Eliashberg function $\alpha^2F(\omega)$ from which to calculate the T_c using the Allen-Dynes-McMillan formula. The maximum T_c was found to be pinned to the minimum phonon frequency as has been observed and discussed in many classes of materials [1,28].

The phonon mechanism of superconductivity for Cu_xTiSe_2 is not at odds with the excitonic insulator picture of the CDW state. Note that the excitonic and lattice instabilities should appear simultaneously as reported by Kogar *et al.* because they have the same spatial symmetry [51,53]. Within this picture, the excitonic instability drives the CDW formation of the $2 \times 2 \times 2$ periodic lattice distortion. Then, the CDW must be accompanied by the soft phonon mode of the wave vector L at the CDW quantum critical point. The critical temperature T_c becomes maximum at the minimum phonon frequency within the Eliashberg formalism as we obtained here [28]. The superconductivity is a phonon mediated conventional pairing and the proximity of the maximal superconductivity and the CDW quantum critical point is not coincidental.

ACKNOWLEDGMENTS

We acknowledge valuable discussions with Hyoung Joon Choi on the virtual crystal approximation. This work was supported by the National Research Foundation of Korea under NRF-2020R1I1A1A01054852 (THP) and NRF-2021R1F1A1A063697 (HYC).

- [1] L. R. Testardi, Structural instability and superconductivity in A-15 compounds, *Rev. Mod. Phys.* **47**, 637 (1975).
- [2] T. Kiss, T. Yokoya, A. Chainani, S. Shin, T. Hanaguri, M. Nohara, and H. Takagi, Charge-order-maximized momentum-dependent superconductivity, *Nat. Phys.* **3**, 720 (2007).
- [3] B. Loret, N. Auvray, Y. Gallais, M. Cazayous, A. Forget, D. Colson, M.-H. Julien, I. Paul, M. Civelli, and A. Sacuto, Intimate link between charge density wave, pseudogap and superconducting energy scales in cuprates, *Nat. Phys.* **15**, 771 (2019).
- [4] Y.-X. Jiang, J.-X. Yin, M. M. Denner, N. Shumiya, B. R. Ortiz, G. Xu, Z. Guguchia, J. He, Md. S. Hossain, X. Liu *et al.*, Unconventional chiral charge order in kagome superconductor KV_3Sb_5 , *Nat. Mater.* **20**, 1353 (2020).
- [5] M. R. Otto, J.-H. Pöhls, L. P. René de Cotret, M. J. Stern, M. Sutton, and B. J. Siwick, Mechanisms of electron-phonon coupling unraveled in momentum and time: The case of soft phonons in $TiSe_2$, *Sci. Adv.* **7**, abf2810 (2021).
- [6] B. Keimer, S. A. Kivelson, M. R. Norman, S. Uchida, and J. Zaanen, From quantum matter to high-temperature superconductivity in copper oxides, *Nature (London)* **518**, 179 (2015).
- [7] K. Hashimoto, K. Cho, T. Shibauchi, S. Kasahara, Y. Mizukami, R. Katsumata, Y. Tsuruhara, T. Terashima, H. Ikeda, M. A. Tanatar *et al.*, A sharp peak of the zero-temperature penetration depth at optimal composition in $BaFe_2(As_{1-x}P_x)_2$, *Science* **336**, 1554 (2012).
- [8] D. N. Basov and A. V. Chubukov, Manifesto for a higher T_c , *Nat. Phys.* **7**, 272 (2011).
- [9] N. D. Mathur, F. M. Grosche, S. R. Julian, I. R. Walker, D. M. Freye, R. K. W. Haselwimmer, and G. G. Lonzarich, Magnetically mediated superconductivity in heavy fermion compounds, *Nature (London)* **394**, 39 (1998).
- [10] F. Steglich, J. Aarts, C. D. Bredl, W. Lieke, D. Meschede, W. Franz, and H. Schäfer, Superconductivity in the Presence of Strong Pauli Paramagnetism: $CeCu_2Si_2$, *Phys. Rev. Lett.* **43**, 1892 (1979).
- [11] E. Morosan, H. W. Zandbergen, B. S. Dennis, J. W. G. Bos, Y. Onose, T. Klimczuk, A. P. Ramirez, N. P. Ong, and R. J. Cava, Superconductivity in Cu_xTiSe_2 , *Nat. Phys.* **2**, 544 (2006).
- [12] A. F. Kusmartseva, B. Sipos, H. Berger, L. Forró, and E. Tutiš, Pressure Induced Superconductivity in Pristine $1T-TiSe_2$, *Phys. Rev. Lett.* **103**, 236401 (2009).
- [13] Y. Feng, J. Wang, R. Jaramillo, J. van Wezel, S. Haravifard, G. Srajer, Y. Liu, Z.-A. Xu, P. B. Littlewood, and T. F. Rosenbaum, Order parameter fluctuations at a buried quantum critical point, *Proc. Natl. Acad. Sci. USA* **109**, 7224 (2012).
- [14] B. Wang, Y. Liu, X. Luo, K. Ishigaki, K. Matsubayashi, W. Lu, Y. Sun, J. Cheng, and Y. Uwatoko, Universal phase diagram of superconductivity and charge density wave versus high hydrostatic pressure in pure and Se-doped $1T-TaS_2$, *Phys. Rev. B* **97**, 220504(R) (2018).
- [15] Z. Chi, X. Chen, F. Yen, F. Peng, Y. Zhou, J. Zhu, Y. Zhang, X. Liu, C. Lin, S. Chu, Y. Li, J. Zhao, T. Kagayama, Y. Ma, and Z. Yang, Superconductivity in Pristine $2H_a-MoS_2$ at Ultrahigh Pressure, *Phys. Rev. Lett.* **120**, 037002 (2018).
- [16] F. J. Di Salvo, D. E. Moncton, and J. V. Waszczak, Electronic properties and superlattice formation in the semimetal $TiSe_2$, *Phys. Rev. B* **14**, 4321 (1976).
- [17] S. Kitou, A. Nakano, S. Kobayashi, K. Sugawara, N. Katayama, N. Maejima, A. Machida, T. Watanuki, K. Ichimura, S. Tanda, T. Nakamura, and H. Sawa, Effect of Cu intercalation and pressure on excitonic interaction in $1T-TiSe_2$, *Phys. Rev. B* **99**, 104109 (2019).
- [18] H. Barath, M. Kim, J. F. Karpus, S. L. Cooper, P. Abbamonte, E. Fradkin, E. Morosan, and R. J. Cava, Quantum and Classical Mode Softening Near the Charge-Density-Wave-Superconductor Transition of Cu_xTiSe_2 , *Phys. Rev. Lett.* **100**, 106402 (2008).
- [19] J. A. Holy, K. C. Woo, M. V. Klein, and F. C. Brown, Raman and infrared studies of superlattice formation in $TiSe_2$, *Phys. Rev. B* **16**, 3628 (1977).
- [20] J. F. Zhao, H. W. Ou, G. Wu, B. P. Xie, Y. Zhang, D. W. Shen, J. Wei, L. X. Yang, J. K. Dong, M. Arita, H. Namatame, M. Taniguchi, X. H. Chen, and D. L. Feng, Evolution of the Electronic Structure of $1T-Cu_xTiSe_2$, *Phys. Rev. Lett.* **99**, 146401 (2007).
- [21] Y. Joe, X. M. Chen, P. Ghaemi, K. D. Finkelstein, G. A. de la Peña, Y. Gan, J. C. T. Lee, S. Yuan, J. Geck, G. J. MacDougall, T. C. Chiang, S. L. Cooper, E. Fradkin, and P. Abbamonte, Emergence of charge density wave domain walls above the superconducting dome in $1T-TiSe_2$, *Nat. Phys.* **10**, 421 (2014).
- [22] M. Calandra and F. Mauri, Charge-Density Wave and Superconducting Dome in $TiSe_2$ from Electron-Phonon Interaction, *Phys. Rev. Lett.* **106**, 196406 (2011).
- [23] D. Qian, D. Hsieh, L. Wray, E. Morosan, N. L. Wang, Y. Xia, R. J. Cava, and M. Z. Hasan, Emergence of Fermi Pockets in a New Excitonic Charge-Density-Wave Melted Superconductor, *Phys. Rev. Lett.* **98**, 117007 (2007).
- [24] S. Y. Li, G. Wu, X. H. Chen, and L. Taillefer, Single-Gap s -Wave Superconductivity near the Charge-Density-Wave Quantum Critical Point in Cu_xTiSe_2 , *Phys. Rev. Lett.* **99**, 107001 (2007).
- [25] A. Kogar, G. A. de la Pena, S. Lee, Y. Fang, S. X.-L. Sun, D. B. Lioi, G. Karapetrov, K. D. Finkelstein, J. P. C. Ruff, P. Abbamonte, and S. Rosenkranz, Observation of a Charge Density Wave Incommensuration Near the Superconducting Dome in Cu_xTiSe_2 , *Phys. Rev. Lett.* **118**, 027002 (2017).
- [26] M. Maschek, S. Rosenkranz, R. Hott, R. Heid, M. Merz, D. A. Zocco, A. H. Said, A. Alatas, G. Karapetrov, S. Zhu, J. van Wezel, and F. Weber, Superconductivity and hybrid soft modes in $TiSe_2$, *Phys. Rev. B* **94**, 214507 (2016).
- [27] R. Ganesh, G. Baskaran, J. van den Brink, and D. V. Efremov, Theoretical Prediction of a Time-Reversal Broken Chiral Superconducting Phase Driven by Electronic Correlations in a Single $TiSe_2$ Layer, *Phys. Rev. Lett.* **113**, 177001 (2014).
- [28] J. E. Moussa and M. L. Cohen, Two bounds on the maximum phonon-mediated superconducting transition temperature, *Phys. Rev. B* **74**, 094520 (2006).
- [29] P. Giannozzi, S. Baroni, N. Bonini, M. Calandra, R. Car, C. Cavazzoni, D. Ceresoli, G. L. Chiarotti, M. Cococcioni, I. Dabo *et al.*, QUANTUM ESPRESSO: A modular and open-source software project for quantum simulations of materials, *J. Phys.: Condens. Matter* **21**, 395502 (2009).
- [30] J. P. Perdew and A. Zunger, Self-interaction correction to density-functional approximations for many-electron systems, *Phys. Rev. B* **23**, 5048 (1981).
- [31] D. R. Hamann, Optimized norm-conserving Vanderbilt pseudopotentials, *Phys. Rev. B* **88**, 085117 (2013).
- [32] H. J. Monkhorst and J. D. Pack, Special points for Brillouin-zone integrations, *Phys. Rev. B* **13**, 5188 (1976).

- [33] N. Marzari, D. Vanderbilt, A. De Vita, and M. C. Payne, Thermal Contraction and Disorder of the Al(110) Surface, *Phys. Rev. Lett.* **82**, 3296 (1999).
- [34] N. J. Ramer and A. M. Rappe, Virtual-crystal approximation that works: Locating a compositional phase boundary in $\text{Pb}(\text{Zr}_{1-x}\text{Ti}_x)\text{O}_3$, *Phys. Rev. B* **62**, R743 (2000).
- [35] L. Bellaiche and D. Vanderbilt, Virtual crystal approximation revisited: Application to dielectric and piezoelectric properties of perovskites, *Phys. Rev. B* **61**, 7877 (2000).
- [36] R. A. Jishi and H. M. Alyahyaei, Electronic structure of superconducting copper intercalated transition metal dichalcogenides: First-principles calculations, *Phys. Rev. B* **78**, 144516 (2008).
- [37] S. Kitou, S. Kobayashi, T. Kaneko, N. Katayama, S. Yunoki, T. Nakamura, and H. Sawa, Honeycomb lattice type charge density wave associated with interlayer Cu ions ordering in $1T\text{-Cu}_x\text{TiSe}_2$, *Phys. Rev. B* **99**, 081111(R) (2019).
- [38] Z. Muhammad, K. Mu, H. Lv, C. Wu, Zia ur Rehman, M. Habib, Z. Sun, X. Wu, and L. Song, Electron doping induced semiconductor to metal transitions in ZrSe_2 layers via copper atomic intercalation, *Nano Res.* **11**, 4914 (2018).
- [39] P. V. C. Medeiros, P. S. Stafström, and J. Björk, Effects of extrinsic and intrinsic perturbations on the electronic structure of graphene: Retaining an effective primitive cell band structure by band unfolding, *Phys. Rev. B* **89**, 041407(R) (2014).
- [40] P. V. C. Medeiros, S. S. Tsirkin, Paulo S. Stafström, and J. Björk, Unfolding spinor wave functions and expectation values of general operators: Introducing the unfolding-density operator, *Phys. Rev. B* **91**, 041116(R) (2015).
- [41] S. Baroni, S. de Gironcoli, A. Dal Corso, and P. Giannozzi, Phonons and related crystal properties from density-functional perturbation theory, *Rev. Mod. Phys.* **73**, 515 (2001).
- [42] F. Giustino, M. L. Cohen, and S. G. Louie, Electron-phonon interaction using Wannier functions, *Phys. Rev. B* **76**, 165108 (2007).
- [43] J. Noffsinger, F. Giustino, B. D. Malone, D. Brad, C.-H. Park, S. G. Louie, and M. L. Cohen, EPW: A program for calculating the electron-phonon coupling using maximally localized Wannier functions, *Comput. Phys. Commun.* **181**, 2140 (2010).
- [44] P. B. Allen, Neutron spectroscopy of superconductors, *Phys. Rev. B* **6**, 2577 (1972).
- [45] W. L. McMillan, Transition temperature of strong-coupled superconductors, *Phys. Rev.* **167**, 331 (1968).
- [46] P. B. Allen and R. C. Dynes, Transition temperature of strong-coupled superconductors reanalyzed, *Phys. Rev. B* **12**, 905 (1975).
- [47] Y. Takaoka and K. Motizuki, Lattice dynamics of $1T\text{-TiSe}_2$, *J. Phys. Soc. Jpn.* **49**, 1838 (1980).
- [48] S. S. Jaswal, Lattice dynamics of TiSe_2 , *Phys. Rev. B* **20**, 5297 (1979).
- [49] S. S. Jaswal, Phonons and charge density waves in $1T\text{-TiSe}_2$, *Solid State Commun.* **28**, 923 (1978).
- [50] H. Tornatzky, R. Gillen, H. Uchiyama, and J. Maultzsch, Phonon dispersion in MoS_2 , *Phys. Rev. B* **99**, 144309 (2019).
- [51] J. M. Bok, J. Hwang, and H.-Y. Choi, Excitonic insulator emerging from semiconducting normal state in $1T\text{-TiSe}_2$, *Phys. Rev. B* **103**, 205108 (2021).
- [52] S. Lee, T. B. Park, J. Kim, S.-G. Jung, W. K. Seong, N. Hur, Y. Luo, D. Y. Kim, and T. Park, Tuning the charge density wave quantum critical point and the appearance of superconductivity in TiSe_2 , *Phys. Rev. Research* **3**, 033097 (2021).
- [53] A. Kogar, M. S. Rak, S. Vig, A. A. Husain, F. Flicker, Y. I. Joe, L. Venema, G. J. MacDougall, T. C. Chiang, E. Fradkin, J. van Wezel, and P. Abbamonte, Signatures of exciton condensation in a transition metal dichalcogenide, *Science* **358**, 1314 (2017).